Published in final edited form as:
Int J Mass Spectrom. 2016 June 1; 403: 15–26. doi:10.1016/j.ijms.2016.02.003.

Refinement of high precision Ru isotope analysis using negative thermal ionization mass spectrometry

K.R. Bermingham*, **R.J. Walker**, and **E.A. Worsham**
Department of Geology, University of Maryland, College Park, MD 20742, USA

Abstract

A refined method for the isolation, purification, and high precision measurement of Ru isotope compositions in natural samples by negative thermal ionization mass spectrometry (N-TIMS) is reported. After chemical purification of Ru using ion exchange chromatography and microdistillation techniques, the Ru isotopic composition is measured as RuO_3^- via N-TIMS. Data are corrected for oxide interferences using the simultaneously measured oxygen isotope composition, and subsequently for mass fractionation using an exponential law. Repeat analyses of an *Alfa Aesar* Ru standard solution demonstrate external reproducibility of $^{100}Ru/^{101}Ru$ to ±6.4 ppm (2SD). This level of precision is more than two times better than prior techniques. Repeat analyses of gravimetrically prepared mixtures of a natural *Alfa Aesar* Ru standard and a ^{100}Ru enriched spike show that isotopic differences of ≥13 ppm can be resolved by single measurements of a material using this method. Repeat analyses of diverse terrestrial materials (chromitites and Os-Ir-Ru alloys) are characterized by compositions that are identical to the *Alfa Aesar* standard, and the external reproducibility for these materials is also identical to that of the chemically pure standard, demonstrating that chemical separation/purification methods introduce no bias to the analysis. These materials likely define the Ru isotopic composition of the Earth's mantle.

Keywords

Ruthenium isotope; ^{100}Ru; Thermal ionization mass spectrometry; N-TIMS

1. Introduction

Mass-independent nucleosynthetic isotopic anomalies have been observed in Ru present in whole rock meteorites and their components [1–7]. The nature and magnitude of the anomalies have been used to investigate the stellar origins of matter in our solar system, as well as nebular mixing processes. Ruthenium isotopes (^{96}Ru = 5.52%; ^{98}Ru = 1.87%; ^{99}Ru = 12.8%; ^{100}Ru = 12.6%; ^{101}Ru = 17.1%; ^{102}Ru = 31.6%; ^{104}Ru = 18.6%) are well suited for this task. This is because of the diverse nucleosynthetic processes by which Ru isotopes were made (*p*-, *s*-, *r*-process; [33]), and the high condensation temperature of Ru (T_c = 1565 K, where T_c is the temperature at which 50% of the element is condensed; [8]). Additionally, there are two short-lived chronometers associated with the Ru isotope system, ^{98}Tc-^{98}Ru and ^{99}Tc-^{99}Ru ($t_{1/2}$ = 4.2–10 Ma and $t_{1/2}$ = 0.21 Ma, respectively; [9]). Conclusive evidence

*Corresponding author. Tel.: +(301) 405-2707. kberming@umd.edu (K.R. Bermingham).

for either chronometer, however, is yet to be identified. Further, given the variations in Ru isotopic compositions among early solar system materials, Ru isotopes show great promise for providing genetic fingerprints of diverse, late-stage accretionary additions to the Earth and Moon [10, 11]. This is possible because the Ru present in, for example, lunar impact melt rocks produced by basin-forming events, is primarily derived from the impactor (e.g., [12]).

High precision isotopic analytical capability is required to fully pursue these cosmochemical and geochemical objectives. Ruthenium isotopes have previously been measured using either thermal ionization mass spectrometry (TIMS; [6, 13]) or multiple-collector inductively coupled plasma mass spectrometry (MC-ICP-MS; e.g., [7, 14]). The current state-of-the-art for $^{100}Ru/^{101}Ru$ is ±31 ppm using TIMS [6] and ±13 ppm using (MC-ICP-MS [7]), where uncertainties are 2SD, defined by repeat analyses of laboratory standards. Here, we present refined chemical and mass spectrometric procedures to precisely measure Ru isotopic compositions in natural samples. The new method offers a better than twofold improvement in precision for some Ru ratios, compared to the existing techniques.

2. Methods

2.1. Samples

The in house laboratory standard used in this study was a Ru *Alfa Aesar Specpure*® plasma standard solution (1000 μg/ml, $RuCl_3$ in 20% HCl). In order to confirm that our chemical isolation/purification and measurement procedures did not impart systematic biases, as well as to define the Ru isotopic composition of modern terrestrial mantle, chromitites from the 492 Ma Shetland ophiolite complex [15] and Os-Ir-Ru alloy grains from the 162 Ma Josephine ophiolite complex [16] were analyzed (EA1). In order to test the procedures for cosmochemical materials, and to enable comparisons of data with data from prior studies, the group IVB iron meteorite Hoba was also analyzed (EA1). Each sample type has a chemically distinct matrix, thus making this suite well suited to testing the robustness of our chemical separation and mass spectrometric protocols.

2.2. Sample preparation

Chromitites (C1, C2, C3) were cut into 2–3 g pieces using a *MK Diamond Products* (Inc.) water-cooled tile saw with a 25.4 cm diameter diamond blade. The pieces were abraded using silicon car-bide sandpaper, in order to remove visible saw marks, rinsed with distilled water, and then fragmented into 0.1–0.5 g chips using a hammer wrapped in plastic film. The fragments were then carefully ground to a fine (~10 μm) powder using an agate mortar and pestle dedicated to chromitites and other terrestrial rocks with high Ru abundances. Between samples, the mortar and pestle were mechanically cleaned by grinding multiple aliquots of silica grains, using new aliquots of silica grains each time. The mortar and pestle were then cleaned in dilute *aqua regia* overnight at ~40 °C, followed by a few hours in *Milli-Q* (water deionized to a resistivity of 18.2 MΩcm) at the same temperature. The Os-Ir-Ru alloy grains analyzed here are a small subset of the grains studied in [16]. No sample preparation prior to digestion was required. Approximately 10 g of the meteorite Hoba was obtained from the Smithsonian Institution National Museum of Natural History (USNM

6506). The sample was cut into a 0.7 g piece using a distilled water-cooled *Leco* "*Vari-cut*" saw with a 12.7 cm diamond wafering blade. The blade was cleaned with carborundum before cutting the sample (as detailed in [17]). Pieces with or near fusion crust and rust patches were avoided. The cut sample was abraded using silicon carbide sandpaper, and then sonicated in *Milli-Q* water three times for 10 min at a time, using fresh *Milli-Q* water each stage. This was done to remove any adhering material from the sample.

2.3. Sample digestion

The Carius tube digestion technique employed to digest chromitites and Os-Ir-Ru alloys is based on the method adapted by [18]. Between 0.9 and 1.2 g of a powdered chromitite sample, or a single Os-Ir-Ru alloy grain (0.05–0.1 g), 3 ml of quartz-distilled concentrated hydrochloric acid (HCl) and 6 ml of quartz-distilled concentrated nitric acid (HNO_3) were placed in a chilled, thick-walled *Pyrex*® Carius tube. The distilled acids were made from either *Sigma Aldrich*® ACS grade or *BDH Aristar*® ACS grade commercial acids. The Carius tube was sealed promptly after addition of the acids in order to avoid possible loss of volatile RuO_4 (boiling point (BP) = 40 °C; [19]), which is produced on the addition of an oxidizing agent to a sample. Digestions of the samples were performed at 240 °C for 4–5 days. Although not critical here, complete dissolution of the sample was typically not achieved. After digestion, the Carius tube was chilled in an ice bath, opened, and the acid phase was transferred to a 60 ml *Savillex* Teflon® beaker containing ~20 ml of quartz-distilled 6 M HCl. The mixed solution was gently dried down to ~2 ml using an ultraviolet heat lamp. The solution from the Carius tube was mixed with the 6 M HCl to promote the reduction of the volatile RuO_4 to a non-volatile form, thus reducing its loss during evaporation. The gentle and incomplete dry down at this stage also limited the loss of RuO_4. Approximately 5 ml of 6 M quartz-distilled HCl was added to the beaker to continue converting the Ru in solution to a chloride form. This solution was gently evaporated down to ~1 ml of residual solution. This step was repeated once.

At this point, Os-Ir-Ru alloy samples were dried down to ~0.2 ml and transferred to the cap of a 5 ml conical bottom *Savillex* Teflon® beaker for microdistillation, as described below. The Ru present in the chromitite samples, however, required further purification before microdistillation, and this was achieved by separating the Ru from the matrix via ion exchange chromatography. In preparation for this, the remaining ~1 ml of solution was evaporated down to a slurry using the heat lamp, after which 5 ml of 0.15 M quartz-distilled HCl was added. This solution was again evaporated to slurry, subsequently taken up in 10 ml of 0.15 M quartz-distilled HCl, and left to dissolve at room temperature. The sample was then transferred to a 10 ml centrifuge tube and centrifuged for 10 minutes at 7000 rpm. The supernatant was then removed for ion exchange chromatography.

The sanded and sonicated meteorite piece was added to 30 ml of 9 M quartz-distilled HCl in a 60 ml *Savillex* Teflon® beaker and left capped at 130 °C on a hotplate for 12 h to digest. Following this, another 20 ml of 9 M quartz-distilled HCl was added to the beaker. The beaker was sonicated for 10 min, and then returned to the hot-plate and left at 150 °C for 24 h. After this treatment, the sample was completely dissolved. The sample was then gently evaporated to slurry, after which 5 ml of 0.15 M HCl was added, and the solution again

slowly evaporated to slurry. The slurry was taken up in 5 ml of 0.15 M quartz-distilled HCl and left to dissolve at room temperature. The sample was transferred to a 10 ml centrifuge tube and centrifuged for 10 min at 7000 rpm. Finally, the supernatant was removed for ion exchange chromatography.

2.4. Ion exchange chromatography

Ruthenium has commonly been isolated using one- or two-stage ion exchange chromatographic procedures and then further purified using microdistillation [6, 7, 20]. Consistently achieving high recovery and high purity Ru with these techniques has been problematic. This is mainly due to the tendency of Ru to exist in multiple oxidation states (0 to +8; [21]), many of which exhibit different redox potentials and cation/anion exchange behaviors. This can lead to loss of Ru during chemical purification, as well as variable efficiency of chromatographic separations and microdistillation.

In this study, a two-step ion exchange chromatographic procedure was initially adapted from previous studies (e.g., [6, 20]), in order to isolate Ru from the large amount (~1 g) of sample matrix used for chromitite and meteorite analyses. This method works by removing the majority of chromium (chromitites) or iron (iron meteorites) from the Ru and other highly siderophile elements (HSE: Re, Os, Ir, Pt, Rh, Pd, Au), in a primary (1°) cation column using an HCl-based chemistry. Ruthenium is separated from the other HSE using a secondary (2°) anion column, and an HCl-HNO_3 based chemistry (Table 1). The yields, however, from the 2° column were only ~50%. This is likely a result of on-column reduction and retention of Ru-complexes in different oxidation states during the elution protocol, in addition to the loss of some RuO_4 during evaporation of the Ru-Re fraction (HNO_3). Subsequently, for those samples requiring column chromatography, better Ru yields were achieved by proceeding directly from the 1° column chemistry to a microdistillation.

In detail, the 1° column cation exchange chromatography used ~10 ml of pre-cleaned *Eichrom* AG50WX8 200–400 mesh cation exchange resin equilibrated in *Milli-Q* water (see EA2 for pre-cleaning steps and Table 1 for elution protocol). This resin was transferred to a *Biorad column* (1.5 cm × 12 cm) as a slurry, then further cleaned using 4× 10 ml 6 M HCl (quartz distilled). The columns were then equilibrated using 10 ml 0.15 M HCl. Each sample was split into two to four 2.5 ml aliquots, and each aliquant (2.5 ml0.15 M HCl) was loaded onto a separate column, such that each column was used to process ~250 mg of sample. The HSE are not retained on the cation exchange column in low molarity HCl, in contrast to the major elements (e.g., Cr^{+3}, Fe^{+2}, Fe^{+3}; [22]). Thus, the HSE were directly collected in 8 ml of 0.15 M HCl after loading. The matrix, which largely remains on the column after HSE elution, was subsequently eluted using 30 ml 6 M HCl. Recovery of HSE per column was >90%. The total procedural blank for Carius tube digestion and 1° column chemistry was 110 ± 63 pg ($n = 4$). The total procedural blank for digestion in *Savillex* Teflon® beakers and 1° column chemistry was 6.1 pg ($n = 1$). These blanks are ≪1% of the total Ru measured for each sample here, and are inconsequential for the measurements reported.

The 2° column utilized anion exchange chromatography to separate Ru from the other HSE. It is based on methods described in[20]. Approximately 3.8 ml of pre-cleaned *Eichrom* AG1X8 anion exchange resin (200–400 mesh; see EA2 for pre-cleaning procedure and Table

1 for elution protocol) equilibrated in *Milli-Q* water was transferred to a *Biorad* column (0.8 cm × 4 cm) as a slurry and further cleaned using 20 ml concentrated HNO_3, 10 ml *Milli-Q* water, 10 ml concentrated HCl, and finally 10 ml of *Milli-Q* water. The resin was then washed using 3 ml of 1 M HCl, and equilibrated using 4 ml of 1 M HCl prior to sample loading. One sample was processed per anion column. Samples were loaded onto the anion resin in 1 ml of 1 M HCl. Matrix elements (and Mo) were rinsed from the resin using 2 ml of 0.5 M HCl and 0.5 ml of 0.8 M HNO_3. Zinc, Cd, and traces of Mo were then eluted using 5 ml of 0.8 M HNO_3. Rhenium and Ru were then eluted together using 10 ml of 8 M HNO_3 and 4 ml concentrated (14 M) HNO_3. Recovery of Ru for this column was ~50%. The total procedural blank for digestion and 2° column chemistry was 28 ± 21 pg (n = 7). This blank is ≪1% of the total Ru measured for each sample here inconsequential for the measurements reported here.

2.5. Microdistillations

Following ion exchange chromatography, Ru was purified by microdistillation. This technique was originally developed to purify Os [23, 24], however, given the similarity in volatility of high valence RuO_4 (BP = 40 °C; [19]) and OsO_4 (BP = 129.7 °C; [19]), this technique can also be used to purify Ru and remove organics which may be present following column chromatography [25]. Here, microdistillations were conducted in 5 ml conical bottom *Savillex* Teflon® vessels, where the sample and oxidant were placed on the cap and a reductant held in the tip of the beaker. Initially, the distillation vessel was placed in a steel block with a stainless steel jacket placed around the body of the beaker. This left the tip of the beaker exposed to the atmosphere to promote warming and oxidation of Ru in the lower part of the vessel, while keeping the top part of the beaker cool to promote reduction of RuO_4. This design, however, was not found to improve recovery yields and was abandoned.

A significant issue in the microdistillation of Ru is achieving consistently high yields. Efficient distillation of Ru requires a strong oxidant to oxidize the Ru, and a strong reductant to reduce the captured Ru in the trap solution. In an effort to improve the recovery of purified Ru, a number of different oxidants and reductants, distillation temperatures, and distillation reaction times were tried. Oxidizing reagents tested for microdistillations included acidified ceric sulfate and acidified (sulfuric acid) dichromic acid ($H_2Cr_2O_7$), and reducing (trapping) reagents included concentrated double quartz distilled hydrobromic acid (HBr), 6 M HCl-ethanol (50:50), and 6 M HCl. Different combinations of the reagents listed above were tested at temperatures ranging from ca. 25 °C to 120 °C for periods between 2 h and 48 h.

The 6 M HCl-ethanol mixture for trapping and reducing Ru resulted in very low recovery yields (<5%), regardless of the oxidant and temperature used. Ceric sulfate also produced poor recovery yields for Ru (<5%) regardless of the trapping/reductant solution and temperature. Acidified $H_2Cr_2O_7$ generally resulted in a higher recovery for Ru (20–90%) that was highly dependent on the trapping/reductant solution used, as well as the reaction time and temperature. It was found that recovery of Ru was low when the oxidation step was carried out at >100 °C. Concentrated HBr as the trapping solution, in combination with

$H_2Cr_2O_7$ as the oxidant resulted in highly variable yields (20–80%). The use of 55 μl of $H_2Cr_2O_7$ as the oxidant and 10 μl of 6 M HCl as the trapping agent consistently produced the highest Ru recovery (50–90%) when distillation was performed at 55 °C for 12 h, and repeated for another 12 h after the addition of an additional 20 μl of $H_2Cr_2O_7$ and replenishment of the 6 M HCl trapping agent. The blank for this microdistillation was 570 ± 160 pg (n = 4). This blank is ≪1% of the total Ru measured for each sample here and inconsequential for the measurements reported. The cause of persistent variability in yields from microdistillation remains unclear, but yields appear to be improved if little matrix remains after the 1° column, and if the sample has been gently and not completely dried down at any stage of the purification chemistry. Importantly, the variability in Ru yield that is observed in this study (20–90%) does not have a significant effect on the isotopic composition measured. Samples which had yields of ~20% generated the same $^{100}Ru/^{101}Ru$ as the same sample with ~90% yields, within the analytical error.

Chromium contamination in the distilled Ru occasionally occurred during the early stages of development of this method, likely due to splashing of $H_2Cr_2O_7$ during distillation. The presence of minor Cr-contamination led to a substantial reduction of the RuO_3^- signal during N-TIMS analysis. Avoidance of Cr-contamination was achieved by slowly heating-up the microdistillation vessel in steps of 10 °C from room temperature. Traces of Os can co-distil with the Ru; however, this contamination of the Ru can be kept to negligible amounts by distilling at ≤55 °C.

Following microdistillation, the purified Ru was ready for loading onto filaments for N-TIMS analysis. Upon completion of the Ru purification, a small aliquot (0.1%) was removed for analysis using an ICP-MS to assess elemental purity and determine the chemical yield of each sample. All samples processed for this study were found to be of high purity with no contamination by potentially interfering elements, such as Zr, Mo, Rh, and Pd.

3. Mass spectrometry

3.1. Instrumentation

A *Thermo-Fisher Triton Plus* TIMS in negative ionization mode was used to make Ru isotope measurements. The analysis of negatively charged molecular species of Ru was refined here from methods reported by [6]. The N-TIMS method has been shown to be a highly sensitive and accurate technique in the analysis of ions with high electron affinities [26]. The instrument was equipped with nine Faraday cups, seven of which were used to measure the seven stable Ru isotopes as trioxides (RuO_3^-) using a single static line measurement method (Fig. 1). High purity oxygen was bled into the source chamber using a variable leak valve to promote formation of RuO_3^-. The oxygen pressure (ranging from 6.50×10^{-7} to 9.60×10^{-7} mbar, depending on the baseline pressure) was allowed to settle at the beginning of the measurement campaign and was left unchanged throughout the session. During development of this method, it was found that within and between run oxygen isotope variations can significantly affect analytical precision. Use of an amplifier equipped with a 10^{12} Ω resistor (connected to the H4 Faraday cup) was employed to measure in-run oxygen isotope compositions by quantifying the $^{104}Ru^{18}O^{16}O_2^-$ species. Possible interferences from ZrO_3^-, MoO_3^-, BaO^-, and PdO_3^- were monitored at masses 138

($^{95}ZrO_3$), 143 ($^{95}MoO_3$), 153 (^{137}BaO), and 156 ($^{108}PdO_3$), using the secondary electron multiplier at the beginning and end of each run. Corrections were neither needed nor applied for these elements.

3.2. Filament preparation and sample loading

Platinum and Re single filaments as well as Ta-Pt and Pt-Pt double filament assemblies were tested. Single Pt filaments generated the most stable and sensitive RuO_3^- signal over the longest periods of time (8–13 h). Prior to loading, the Pt filaments were outgassed in air at 2.2 A for 7–10 min and left for 12–24 h before loading. Different brands of Pt ribbon were tested (EA3), however, all produced similar RuO_3^- signals and levels of precision.

Because of the range of oxidation states of Ru and the markedly different volatilities of these valences, careful attention was paid in maintaining a constant, low valence state during loading. If this is not done, Ru can be present on the filament in both high and low valence states which can lead to different rates of evaporation during warming of the filament (also documented by[13]). This results in unstable and short-lived RuO_3^- signals, as well as complexly fractionated analyses. Different loading solutions (6 M HCl, 6 M HNO_3, concentrated HBr, dilute HBr, Mill-Q) and loading techniques were tried in order to promote a reduced Ru valence state during loading. It was found that gently drying the solution down and then taking it up in concentrated HBr prior to loading on the filament produced the most stable RuO_3^- signals.

Samples containing ~1000 ng Ru were loaded onto the center of a Pt filament. To dry down the Ru solution, the filament was resistively heated by maintaining a current of 0.6 A. Loading in small volumes reduced the probability of the sample spreading on the filament, which can lead to the formation of multiple chemical reservoirs on the filament and signal instability. After the sample solution dried, the current to the filament was gradually increased over a period of ~5 s until it glowed to dull red for ~1 s. This step promoted reduction of the sample on the filament. After glowing the filament, the sample is characterized by a subtle navy colored sheen.

For N-TIMS, samples must typically also be loaded with an activator solution bearing an electron emitter (e.g., [27]). The activator supplies the electrons necessary to form the negatively charged ionic species required. Different electron activators were tried here including silica gel, $Ba(NO_3)_2$, $Ba(NO_3)_2$-NaOH-$Ba(OH)_2$, or NaOH-$Ba(OH)_2$. The most stable, long-lasting signals were obtained by using 0.8–2 μl of NaOH-$Ba(OH)_2$ (super saturated solution), which was painted across the sample (post glowing) with a micro-pipetter tip, while resistively heating the filament using a current of 0.2 A. The activator solution was left to dry at this current, after which the filament was resistively heated to the point that the activator melted across the sample. The Ru loading blank was ≤1 pg and is negligible for the measurements reported here. Filaments were then immediately put into the mass spectrometer.

3.3. Data acquisition protocol

All standards and samples were heated in the mass spectrometer using the same protocol. As documented in earlier studies [6, 13, 28], a temperature maximum was observed, above

which the RuO_3^- signal began to decrease, despite continued heating. Volkening et al. [28] suggested that the drop in signal occurs because the increasing number of RuO_3^- ions formed as a result of the higher reaction rate cannot compensate for the loss of the ions that instantaneously decompose at the higher temperatures. As was also observed by [6], we found that the temperature maximum could not be precisely defined. It appeared to be dependent on the thickness of the filament ribbon and the quality of the load. To avoid the sharp decrease in signal after reaching the temperature threshold, the filament was heated slowly to promote exponential growth of the RuO_3^- signal, and the heating rate gradually tapered off to achieve a stable signal ($^{102}RuO_3^-$ ~0.7 to 1.2 V) at a low and constant heating rate (0.1 Ma/min) during a 13 h measurement period. The RuO_3^- signal generally fell to 0.5–1.0 V during a run (8–13 h). The temperatures of the filament during data collection ranged from 830 °C to 1000 °C, but typically remained between 850 °C and 930 °C, as recorded by a pyrometer.

All measurements were performed using a single line, static acquisition scheme, where the mass 148 beam, corresponding to $^{100}Ru^{16}O_3^-$, was directed into the axial Faraday cup (Fig. 1). The original measurement method using only 10^{11} Ω resistors proceeded as follows: Between 1000 and 1800 ratios were collected with 16.777 s integration times, one integration, 4 s idle times, in blocks of 20 ratios. Between each block, 30 s baseline measurements by beam deflection with a 10 s pre-baseline wait time were made. Inter-amplifier biases were canceled by electronically rotating the amplifiers at the beginning of each block, using the virtual amplifier capability of the *Triton*. Every 3 blocks, the 148 peak was centered and refocused using the automated peak centering and focus capability of the *Triton*.

Upon installation of a 10^{12} Ω resistor, in-run oxygen isotope compositions were monitored by measuring the $^{104}Ru^{18}O^{16}O_2^-$ species in the H4 Faraday cup. The 10^{12} Ω resistor is used to increase the signal to noise ratio measured by the amplifier, when the effective signal strength of the ion beam is between ~1 and 20 mV (e.g.,[29]), a typical intensity of the $^{104}Ru^{18}O^{16}O_2^-$ signal. Two measurement methods tested after the installation of the 10^{12} Ω resistor were characterized either by using 2 integrations (termed *long integration method*), or 1 integration (termed *short integration method*). The *long integration method* is as follows: Between 100–250 ratios were collected with 67.1 s integration times, two integrations, 15 s idle times, in blocks of 25. Inter-amplifier biases were canceled by rotating the amplifiers. The 10^{12} Ω resistor amplifier connected to H4 was excluded from the rotation scheme. The 148 peak was centered and the beam focused using the automated peak centering and focus capability of the *Triton* at the beginning of each block. Twenty minute baseline measurements were made every five blocks for each Faraday cup/amplifier pair by beam deflection, with a 30 s pre-baseline wait time. Longer idle times, pre-baseline wait times, and baseline measurement times were used to accommodate the longer settling time required with usage of the 10^{12} Ω resistor. For the *short integration method*, the number of integrations was reduced to one, the number of ratios increased to 500, ratios were measured in blocks of 10, and baseline measurements occurring every 10 bocks. All the other parameters were kept constant.

To describe measurement results for $^{100}Ru/^{101}Ru$, the ratio for which the best precision is obtained, we use the $\mu^{100}Ru$ notation, which corresponds to the deviation of the $^{100}Ru/^{101}Ru$ of a sample, relative to average isotope ratio calculated for the repeat analysis of the *Alfa Aesar* standard for that analytical campaign, in parts per million:

$$\mu^{100}\mathrm{Ru}_{\mathrm{sample}}\left[\frac{\left(\frac{^{100}\mathrm{Ru}}{^{101}\mathrm{Ru}}\right)_{\mathrm{sample}}}{\left(\frac{^{100}\mathrm{Ru}}{^{101}\mathrm{Ru}}\right)_{\mathrm{standard}}}-1\right]\times 10^{6}$$

3.4. Mass fractionation correction

Instrumental fractionation is the major limiting factor in the accurate determination of isotopic ratios by mass spectrometry. For thermal ionization sources, it is largely influenced by preferential evaporation of light isotopes relative to heavier isotopes. The effect of this mass-dependent fractionation can be corrected for a given isotope ratio $\left(R_y^x\right)$ by normalizing to a second ratio $\left(R_y^w\right)$ of two stable and non-radiogenic isotopes using the exponential law [30]:

$$R_{wy}^{xy}=\left(R_y^x\times M_y^x\right)^{-\beta}$$

where R_{wy}^{xy} corresponds to the mass fractionation corrected ratio, R_y^x is the measured (oxygen corrected) ratio, M_y^x is the atomic mass ratio of the Ru isotope species, and β is the fractionation factor such that:

$$\beta=\frac{\ln\left(R_y^w/R_{y\,true}^w\right)}{\ln\left(M_y^w\right)}$$

where R_y^w is the measured (oxygen corrected) ratio, $R_{y\,true}^w$ is the normalizing ratio ($^{100}Ru/^{101}Ru = 0.745075$; [6]) and R_y^w is the atomic mass ratio of the Ru isotope species.

Mass fractionation using the molecular species, instead of the common isotopic species, was tested. Both correction schemes produced very similar ratios (identical within <2 ppm), but it was found that correction using the isotopic species consistently produced a slightly lower external reproducibility for all Ru isotopes measured, and thus, the isotopic species were used during mass fractionation correction for all data reported here.

Ruthenium comprises seven stable isotopes (^{96}Ru, ^{98}Ru, ^{99}Ru, ^{100}Ru, ^{101}Ru, ^{102}Ru, ^{104}Ru) which provide multiple options for mass fractionation correction. Traditionally $^{100}Ru/^{101}Ru = 0.745075$ has been used [6, 7] and this ratio is applied here. After mass fractionation correction relative to $^{99}Ru/^{101}Ru$, internal precision of 2.5–4.5 ppm (2SE) on $^{100}Ru/^{101}Ru$ is

typically reached by the end of a measurement cycle, consistent with errors predicted by theoretical ion-counting statistics.

3.5. Oxide interferences

The ionization of Ru as RuO_3^- mainly results in the production of $Ru^{16}O_3^-$, but also, in smaller abundances other oxygen species including $Ru^{16}O_2{}^{17}O^-$, $Ru^{16}O^{17}O_2^-$, $Ru^{16}O^{18}O_2^-$, $Ru^{16}O$, ^{17}O, $^{18}O^-$, $Ru^{17}O_3^-$, and $Ru^{17}O_2{}^{18}O^-$. These species result in isobaric interferences on the major Ru isotopes measured that must be corrected for. Additional species ($Ru^{17}O^{18}O_2$ and $Ru^{18}O_3$) are also formed; however, they are in such low abundance that they do not generate significant interferences. The measured intensity at mass x (^{x}I) is derived from the combination of the signal due to the $^{x-48}Ru^{16}O_3$ trioxide, and signals derived from other isobaric Ru trioxides. These oxide interferences must be corrected for in order to obtain precise data. The oxide correction equations developed for Ru and Os isotope measurement by N-TIMS were applied here (e.g., [27, 31]). Three different reduction protocols were tried and these will be discussed in turn:

a. *Nier correction scheme*: Where oxide interference corrections are estimated by assuming that Ru is associated with oxygen with an ambient isotopic composition (*Nier correction*; $^{17}O/^{16}O = 0.0003749$ and $^{18}O/^{16}O = 0.0020439$; [32]). This reduction protocol does not take into account within-run or between-run oxygen isotope variations. The highest external precision obtained here using this reduction scheme, was $\mu^{100}Ru \pm 7.7$, where $n = 48$ (2SD; Table 2, Fig. 2a).

b. *Single measured oxygen value correction scheme*: This reduction protocol employs two iterations to enable the measurement of the within-run oxygen isotope compositions as an average single value for the measurement. First, oxide interference corrections are estimated by assuming that Ru is associated with oxygen with an ambient isotopic composition (*Nier correction*). After correcting the oxygen isotope interferences on the RuO_3 species, we calculated an average $^{18}O/^{16}O$ composition from the $^{104}Ru^{16}O_2{}^{18}O$ species for that measurement. The corresponding $^{17}O/^{16}O$ composition has traditionally been determined by using the terrestrial fractionation line slope ($^{17}O/^{16}O$ vs. $^{18}O/^{16}O = 0.095$, or $\delta\ ^{17}O/^{16}O$ vs. $\delta\ ^{18}O/^{16}O = 0.52$). However, we found that using an iteratively derived slope of $^{17}O/^{16}O$ vs. $^{18}O/^{16}O = 0.47$ ($\mu^{100}Ru \pm 6.4$; 2SD) generated far higher precision than if $^{17}O/^{16}O$ vs. $^{18}O/^{16}O = 0.0954$ ($\mu^{100}Ru > 30$; 2SD) was used. This is either because there is interference on the $^{104}Ru^{16}O_2{}^{18}O$ peak used to calculate $^{18}O/^{16}O$ or because the fractionation of $^{17}O/^{16}O$ and $^{18}O/^{16}O$ during analysis does not follow the terrestrial fractionation trend. Careful monitoring of the $^{104}Ru^{16}O_2{}^{18}O$ peak indicated that there were no interferences on the $^{104}Ru^{16}O_2{}^{18}O$ peak. However, evidence for “non-mass-dependent” fractionation of the $^{17}O/^{16}O$ and $^{18}O/^{16}O$ ratios was found when measuring $^{104}Ru^{16}O_2{}^{17}O$ and $^{104}Ru^{16}O_2{}^{18}O$ of a ^{104}Ru enriched spike solution (EA4). For the analyses of the spike, in situ measurement of $^{17}O/^{16}O$ and $^{18}O/^{16}O$ was achieved by monitoring the $^{104}Ru^{16}O_2{}^{17}O$ species and $^{104}Ru^{16}O_2{}^{18}O$. We found that the $^{17}O/^{16}O$ vs. $^{18}O/^{16}O$ slope varied between runs (0.08 to 0.28; EA4). The deviation of the measured $^{17}O/^{16}O$ vs. $^{18}O/^{16}O$ slope from the

terrestrial fractionation line is potentially a result of mixing of isotopically distinct reservoirs of oxygen from the tank and the filament. To obtain more accurate and precise oxide corrections, the $^{17}O/^{16}O$ ratio should be measured in situ along with the $^{18}O/^{16}O$ species. However, this was not viable for our instrument during typical analyses, given the very small signal intensities associated with $^{96}Ru^{16}O_2{}^{17}O$ (<1 mV). Thus, for the measurements where oxygen was measured in situ, the corresponding $^{17}O/^{16}O$ was calculated using an iteratively derived slope of $^{17}O/^{16}O$ vs. $^{18}O/^{16}O = 0.47$. This oxygen isotope composition was then used in a second iteration after the first iteration *Nier correction* to correct for oxygen isotope interferences on the RuO_3 species. This reduction scheme is referred to as using a *single measured oxygen isotope composition* to correct for oxide interferences on the RuO_3 species. It demonstrates an external reproducibility of $\mu^{100}Ru$ ±6.4 (2SD), where $n = 17$.

c. *Line-by-line oxygen correction scheme*: This reduction scheme similarly employs two iterations. It was designed to monitor the evolution of the oxygen isotope composition during each line. As with (b), the first iteration involved correcting for the oxide interferences by assuming that Ru is associated with oxygen with an ambient isotopic composition (*Nier correction*). The second iteration involves calculating an average $^{18}O/^{16}O$ composition from the $^{104}Ru^{16}O_2{}^{18}O$ species for each line. We then took the oxygen isotope composition associated with that line to correct for oxide interferences on the corresponding RuO_3 species measured in the same line. A slope of 0.47 was used to calculate $^{17}O/^{16}O$, as described above. This reduction scheme is referred to as using a *line-by-line measured oxygen isotope composition to* correct for oxide interferences on the RuO species. It demonstrates a precision $\mu^{100}Ru$ ±6.4 (2SD; Table 3, Fig. 2b), where $n = 17$.

Although the different correction schemes tried here produce similar levels of precision, the highest precision was achieved by using either the line-by-line measured oxygen isotope composition or the single measured oxygen isotope composition to correct for oxide interferences on the RuO_3 species. We consider the line-byline reduction protocol to be preferable because this method can better monitor in-run changes in the oxygen isotope composition. For each reduction scheme, small residual internal correlations between Ru isotopes persist for most isotope ratios. These likely reflect small uncorrected variations in the isotopic composition of oxygen during the course of a run. The measured oxygen isotope composition is likely a combination of the oxygen being bled into the source can, and that provided by the activator (NaOH-$Ba[OH]_2$). Notably, it was found that maintaining a stable oxygen pressure during an analysis and a measurement campaign, in addition to careful application of the same volume of activator to each filament, was essential to reducing the variation in oxygen composition within and between runs.

The precision achieved on the remaining Ru isotopes is significantly worse (>50 ppm) using the measured oxygen composition scheme (b) or (c), compared to (a), although the line-by-line correction scheme produces slightly (<5 ppm) more precise data than the single value correction scheme. For the line-by-line correction scheme, internal weak correlations

between Ru isotope ratios and the oxygen isotope composition ($^{18}O/^{16}O$) persist. For example, a weak positive correlation was occasionally observed for ^{102}Ru vs. $^{18}O/^{16}O$ (r^2 = 0.07) and ^{104}Ru vs. $^{18}O/^{16}O$ (r^2 = 0.13), coupled with a weak negative correlation for ^{96}Ru vs. $^{18}O/^{16}O$ (r^2 = 0.0.05), ^{98}Ru vs. $^{18}O/^{16}O$ (r^2 = 0.11), and ^{100}Ru vs. $^{18}O/^{16}O$ (r^2 = 0.00.06). This correlation varies in both direction and strength depending on the Ru isotope ratio used. The strength and direction of these correlations also vary between runs, but they are of consistently weak nature. For the single value correction scheme, however, between-run Ru isotope ratios strongly correlate with the oxygen isotope composition ($^{18}O/^{16}O$) calculated from the oxide corrected $^{104}Ru^{16}O_2{}^{18}O$ species. For example, positive correlations persist for ^{102}Ru vs. $^{18}O/^{16}O$ (r^2 = 0.91), ^{104}Ru vs. $^{18}O/^{16}O$ (r^2 = 0.87), ^{100}Ru vs. $^{18}O/^{16}O$ (r^2 = 0.0082), and negative correlations persist for ^{96}Ru vs. $^{18}O/^{16}O$ (r^2 = 0.86) and ^{98}Ru vs. $^{18}O/^{16}O$ (r^2 = 0.88).

These correlations confirm in both correction schemes that the changing oxygen isotope composition observed within and between runs can directly and adversely affect the reported Ru isotope composition. The persistence of ^{x}Ru vs. $^{18}O/^{16}O$ correlations indicates that there is an additional effect in the oxygen isotope correction scheme that is currently not adequately accounted for in the measurement and/or reduction protocols. Although not desired, this is not relevant to the aim of this work, which was to measure $^{100}Ru/^{101}Ru$ to <10 ppm (2SD). When the other Ru isotope species are required these ratios can be corrected with the Nier correction scheme. The Nier method generated external reproducibility for short-term measurement campaigns (1 month) of $\mu^{96}Ru$ = 67, $\mu^{98}Ru$ = 138, $\mu^{100}Ru$ = 8.2, $\mu^{102}Ru$ = 35, $\mu^{104}Ru$ = 56 (2SD; Table 3) and is similar to the long-term precision (8 months) $\mu^{96}Ru$ = 61, $\mu^{98}Ru$ = 137, $\mu^{100}Ru$ = 7.7, $\mu^{102}Ru$ = 32, $\mu^{104}Ru$ = 55 (2SD; Table 3, Fig. 2b). These precisions are higher than the precisions reported by [6] of $\mu^{96}Ru$ = 119, $\mu^{98}Ru$ = 198, $\mu^{100}Ru$ = 31, $\mu^{102}Ru$ = 64, $\mu^{104}Ru$ = 58, and are comparable to those obtained using MC-ICPMS ($\mu^{96}Ru$ = 45, $\mu^{98}Ru$ = 52, $\mu^{100}Ru$ = 13, $\mu^{102}Ru$ = 15, $\mu^{104}Ru$ = 31;[7]), but for $\mu^{100}Ru$ which is significantly higher in precision.

3.6. Measurement method integration times

As stated in Section 3.3, two measurement methods were tried during this study. The initial method (*long integration method*) involved setting the number of integrations to two and the number of ratios to 250. The second method involved shortening the integration time (*short integration method*) by changing the number of integrations to one, increasing the number of ratios to 500, ratios were measured in blocks of 10, and baseline measurements occurring every 10 bocks. All of the other parameters were kept constant. The different measurement methods varied the length of time of ion current integration on the Faraday cups.

It was found that the long integration method did not provide sufficient precision to precisely measure the oxygen isotope composition during a run. This was evidenced by the resulting lower level of precision on $\mu^{100}Ru$ ±10 (2SD; n = 19), when using a line-by-line measured oxygen isotopic composition to correct data collected using the long integration, than if an assumed oxygen composition was used (e.g., [32]).

Subsequently, the short integration method was tried and a higher level of precision was reached on $\mu^{100}Ru$ ±6.4 (n = 17; 2SD) using this method than reached using the long

integration times. As the rate of change of the oxygen isotope composition during Ru isotope analysis is rapid, shorter integration times enable more precise oxygen isotope measurement and thus a more precise oxide interference correction.

4. Results and discussion

4.1. Precision of the Ru isotope measurements

The precision of our $^{100}Ru/^{101}Ru$ analysis was monitored by measuring two gravimetrically prepared mixtures (Mix A and Mix B) of Ru standard and ^{100}Ru-enriched spike. The gravimetric predictions of these mixes are $\mu^{100}Ru_A$ = +14.9 ppm and $\mu^{100}Ru_B$ = +29.3 ppm. The spike-standard mixes were processed in the same manner as the Os-Ir-Ru alloys. Separate aliquots of each mix (A and B) were microdistilled once (A1–A2; B1–B3) and measured using different methods as described below.

During testing of the long integration measurement method, a number of spike standard mixes and terrestrial materials were measured (Fig. 3a, EA5). These data were reduced using either an assumed or measured (line-by-line) oxygen composition for the oxide corrections and the isotopic species for mass fractionation correction. For the assumed oxygen composition measurements, repeated measurements of the mixes yielded $\mu^{100}Ru$ = 14.5 ± 3.9 (2SD; Mix A) and $\mu^{100}Ru$ = 27.3 ± 3.2 (2SD; Mix B), which are in excellent agreement with the gravimetric calculation. These data indicate that this measurement scheme and data reduction protocol generate precise data and can resolve differences of <10 ppm.

During the testing of the short integration measurement method, the spike-standard mixes were again measured to confirm precision of the measurement and reduction protocols (Fig. 3b, EA5). These data were reduced using a line-by-line measured oxygen composition for the oxide corrections and the isotopic species for mass fractionation correction. Repeated measurements of the mixes yielded $\mu^{100}Ru$ = 10.7 ± 6.4 (2SD; Mix A) and $\mu^{100}Ru$ = 27.3 ± 3.9 (2SD; Mix B), which are in excellent agreement with the gravimetric calculation. These data indicate that this measurement scheme and data reduction protocols generate precise data and can resolve differences of ≥ 13 ppm.

4.2. Ruthenium isotope measurement of natural samples

The analyses of Ru separated from chromitites from the 492 Ma Shetland ophiolite complex [15], Os-Ir-Ru alloy grains from the 162 Ma Josephine ophiolite complex [16], and the iron meteorite Hoba (IVB), using separate dissolutions and different purification protocols, allowed for the thorough assessment of our methods when applied to natural samples (Table 4, Fig. 4). These data were collected when using the long integration measurement method and thus were corrected using an assumed oxygen isotope composition [32], and mass fractionation corrected using $99Ru/^{101}Ru$ = 0.745075. Repeat analyses of Ru fractions from the chromitites processed through 1° and 2° columns, and microdistillation show good agreement with the Ru standard solution. There is a slight positive offset for $\mu^{100}Ru$ ($\mu^{100}Ru$ +4.73, 2SD), thus one of these samples (C3_02) was reanalyzed using the simplified chemistry (1° column and microdistillation) and showed no statistically significant offset

from the *Alfa Aesar* standard (μ^{100}Ru +0.85, 2SD). This may suggest that the second stage chemistry may add a small bias (<5 ppm) which is at the limit of our analytical precision. Consequently, the simplified chemistry is the preferred method to process samples. The Os-Ir-Ru alloys processed through microdistillation show excellent reproducibility (μ^{100}Ru +0.08 ± 7.6; 2SD) comparable to what is observed for the Ru Alfa Aesar standard solution, with no statistically significant deviation from the terrestrial standard. Analysis of the iron meteorite Hoba, which was passed through 1° and 2° columns, and microdistillation, is in good agreement with published data, but is more precise.

Data for the geological samples were not collected using the preferred analytical method which enables in situ oxygen isotope measurement and oxide interference correction. The excellent agreement between the spike-standard data measured using both measurement methods, however, indicates that both measurement protocols produce very precise data. Thus, the measurements of the natural samples are taken as evidence that our methods of chemical isolation/purification and measurement of Ru do not impart biases. The Ru isotope compositions determined here for chromitites from the 492 Ma Shetland ophiolite complex and Os-Ir-Ru alloy grains from the 162 Ma Josephine ophiolite complex are interpreted to be representative of the Earth's mantle.

5. Conclusions

We have refined the chemical isolation methods and measurement of Ru by N-TIMS using a *Thermo-Fisher* Triton Plus mass spectrometer. Repeat analyses of an *Alfa Aesar* Ru standard solution demonstrate external reproducibility within ±6.4 ppm (2SD) for ^{100}Ru/^{101}Ru using a line-by-line measured oxygen isotope composition to correct for oxide interferences on the RuO_3 species and the isotopic species for mass fractionation correction. Repeat analysis of gravimetrically prepared mixtures of a natural Alfa Aesar Ru standard and a ^{100}Ru enriched spike show that differences of ≥13 ppm can be resolved using this measurement method. Repeat analysis of separate dissolutions of iron meteorites, modern day chromitites, and Os-Ir-Ru alloys demonstrate that the chemical isolation procedures applied do not shift the Ru isotope composition.

Acknowledgements

This work has been supported by the NASA grants NNX13AF83G and NNA14AB07A, and NSF-CSEDI grants EAR1160728 and EAR1265169. These sources of funding are gratefully acknowledged. We would like to thank editor P. Barran and external reviewer F. Corfu for providing thorough and helpful reviews of the original manuscript; I.S. Puchtel for discussions and assistance in the chemistry labs; R.D. Ash for assistance with MC-ICP-MS instruments; and B. O'Driscoll for providing the Shetland ophiolite samples.

Appendix A.

EA1

Samples analyzed and chemical protocol employed.

Sample	Rock type	Ru(μgg^{-1})[a]	Digestion	Isolation/purification[b]	Chemical yields (%)[c]
C1	Chromitite	16.68	Carius tube	1°, 2°, MD	~20
C2	Chromitite	5.908	Carius tube	1°, 2°, MD	~20

Sample	Rock type	Ru(μgg^{-1})[a]	Digestion	Isolation/purification[b]	Chemical yields (%)[c]
C3_01	Chromitite	20.06	Carius tube	1°, 2°, MD	~20
C3_02	Chromitite	20.06	Carius tube	1°, MD	~20
L5-3	Os-Ir-Ru alloy	5.67 wt%	Carius tube	MD	N/A
M3-6	Os-Ir-Ru alloy	14.10 wt%	Carius tube	MD	N/A
M8-2	Os-Ir-Ru alloy	14.66 wt%	Carius tube	MD	N/A
Hoba	IVB iron	29.15	Teflon® beaker	1°, 2°, MD	~20
SS-A[d]	-	-	Carius tube	MD	N/A
SS-B[d]	-	-	Carius tube	MD	N/A

[a] Chromitite data from [15]; Os-Ir-Ru alloy data from [16]; Hoba data from [17].

[b] 1° refers to primary cation column; 2° refers to secondary anion column, MD refers to microdistillation.

[c] Chemical yields from alloy chemistry and spike-standard mix chemistry are unknown due to the unknown quantity of the sample initially digested.

[d] SS-A refers to spike standard mix A; SS-B refers to spike standard mix B.

EA2

Cation and anion exchange column pre-cleaning procedures.

(1) Fill Teflon resin bottle with *Biorad* resin mixed with *Milli-Q* water.

(2) Shake mixture and let resin settle for 15 min

(3) Decant water

(4) Fill with *Milli-Q* water and shake thoroughly; let resin settle and decant water

(5) Repeat twice more with *Milli-Q* water

(6) Repeat with 1 M Hydrochloric acid (quartz distilled)

(7) Repeat with 6 M Hydrochloric acid (quartz distilled)

(8) Repeat with 6 M Hydrochloric acid (quartz distilled)

(9) Repeat with 1 M Hydrochloric acid (quartz distilled)

(10) Repeat 3 times with *Milli-Q* water

(11) Repeat with 1 M Nitric acid (quartz distilled)

(12) Repeat with 6 M Nitric acid (quartz distilled)

(13) Repeat with 6 M Nitric acid (quartz distilled)

(14) Repeat with 1 M Nitric acid (quartz distilled)

(15) Repeat 3 times with *Milli-Q* water

EA3

Selection of Pt ribbons used in this study.

Brand	Purity	Size
ESPI metals	5N	0.001” T × 0.020” W
Materion	99.99%	0.001” T × 0.020” W
Pressed Pt ribbon	99.999%	0.005” W

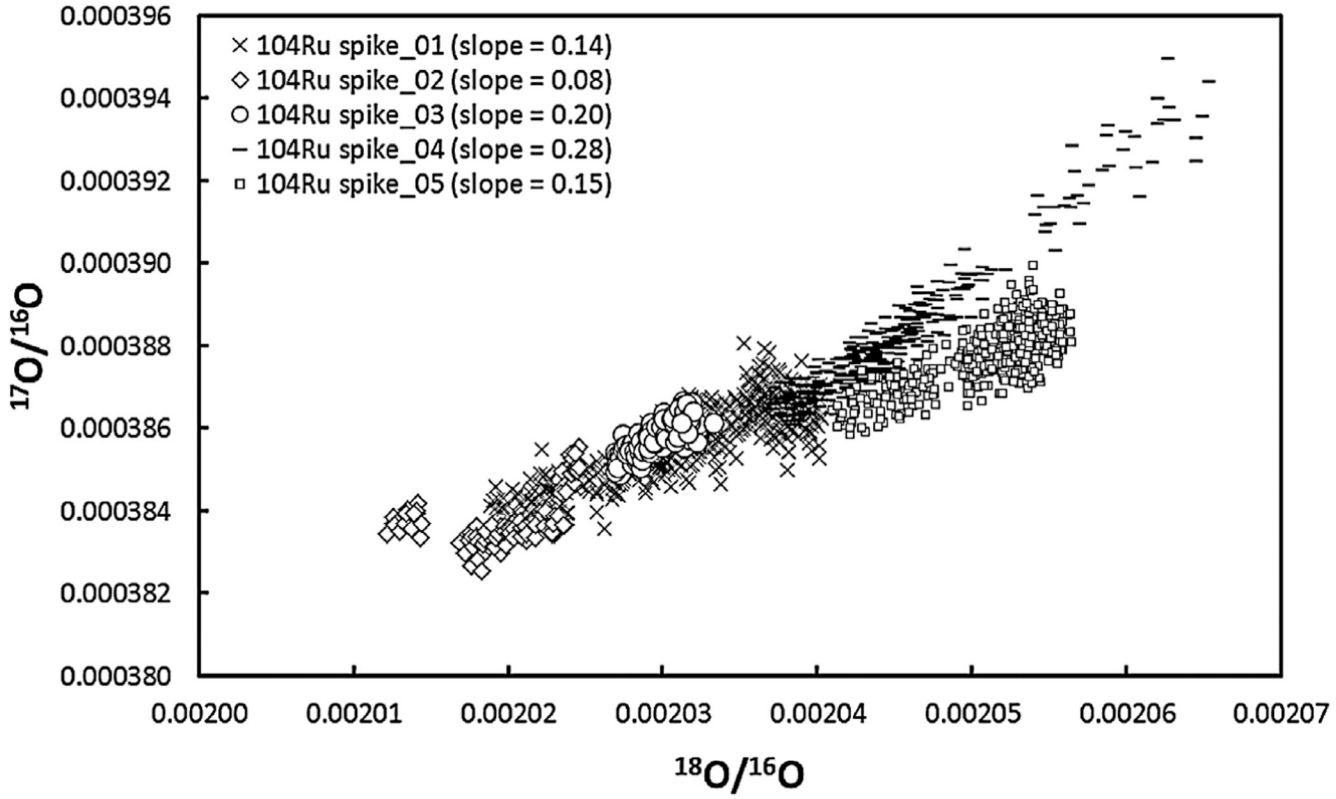

EA4.

Results for the $^{17}O/^{16}O$ and $^{18}O/^{16}O$ measurements for 5 separate analyses of a ^{104}Ru enriched spike solution. These isotope ratios were obtained by measuring $^{104}Ru^{16}O_2{}^{17}O$ and $^{104}Ru^{16}O_2{}^{18}O$. These data have been corrected for oxide interferences using an assumed oxygen isotope composition [32]. The $^{17}O/^{16}O$ vs. $^{18}O/^{16}O$ slopes for each measurement varies from run to run, and moreover, are not in agreement with the slope of the terrestrial fractionation line (0.095). No interferences were identified on either $^{104}Ru^{16}O_2{}^{17}O$ or $^{104}Ru^{16}O_2{}^{18}O$. Thus, the change in slope from run to run and the offset from the terrestrial fractionation line likely indicates a non-mass-dependent fractionation of $^{17}O/^{16}O$ relative to $^{18}O/^{16}O$, as discussed in text.

EA5

Results for the standard-spikes mixes (SS A and SS B). These data have been corrected for oxygen isotope interferences (as indicated) and for mass fractionation using $^{99}Ru/^{101}Ru$ = 0.745075 and the isotopic species. Samples have been compared to the Ru *Alfa Aesar* standard analyses of the respective analytical campaign.

	$^{96/101}Ru$	2SE	$^{98/101}Ru$	2SE	$^{100/101}Ru$	2SE	$^{102/101}Ru$	2SE	$^{104/101}Ru$	2SE
Corrected using an assumed oxygen isotope composition [32]										
SS B1	0.32183	0.000003	0.108954	0.000002	0.737156	0.000003	1.853217	0.000008	1.097482	0.000009
SS B2a	0.321838	0.000004	0.10896	0.000002	0.737155	0.000003	1.853152	0.000009	1.097416	0.00001
SS B2b	0.321824	0.000004	0.108955	0.000002	0.737158	0.000003	1.853212	0.000009	1.097449	0.00001

	$^{96/101}$Ru	2SE	$^{98/101}$Ru	2SE	$^{100/101}$Ru	2SE	$^{102/101}$Ru	2SE	$^{104/101}$Ru	2SE
SS B2c	0.321833	0.000009	0.108962	0.000005	0.737155	0.000005	1.853209	0.000021	1.09748	0.000025
SS B3	0.321816	0.000003	0.108949	0.000002	0.737157	0.000002	1.853216	0.000008	1.097445	0.000007
Mean	0.321828	0.000005	0.108956	0.000002	0.737156	0.000003	1.853201	0.000011	1.097454	0.000012
μ(ppm)	6.9		5.9		27.3		6.5		15.7	
$\pm 2\sigma$(ppm)	54.2		93.0		3.2		29.8		50.3	
SS A1a	0.321821	0.000006	0.108951	0.000003	0.737146	0.000005	1.853225	0.000011	1.09746	0.000014
SS A1b	0.321836	0.000004	0.10896	0.000002	0.737149	0.000002	1.853216	0.000008	1.097461	0.00001
SS A1c	0.321826	0.000004	0.108952	0.000002	0.737145	0.000003	1.853201	0.00001	1.09744	0.000012
SS A1d	0.321823	0.000003	0.108959	0.000002	0.737149	0.000003	1.853208	0.000009	1.097469	0.000009
SS A1e	0.321843	0.000007	0.108968	0.000003	0.737147	0.000006	1.853138	0.000016	1.097425	0.000017
SS A1f	0.321829	0.000004	0.108954	0.000003	0.737146	0.000004	1.853215	0.00001	1.097458	0.00001
A2	0.321822	0.000003	0.108944	0.000002	0.737147	0.000003	1.853249	0.000008	1.09748	0.000009
Mean	0.321829	0.000005	0.108955	0.000002	0.737147	0.000004	1.853208	0.00001	1.097456	0.000012
μ(ppm)	7.23		−2.0		14.5		10.1		17.4	
$\pm 2\sigma$(ppm)	51.0		141.8		3.9		36.9		33.0	
Corrected using a line-by-line measured oxygen isotope composition										
SSB2d	0.321771	0.000003	0.108914	0.000001	0.737165	0.000002	1.85341	0.000008	1.097524	0.000008
SSB2e	0.321795	0.000003	0.108932	0.000002	0.737162	0.000003	1.853323	0.000007	1.097493	0.000008
SSB2f	0.321763	0.000003	0.108911	0.000001	0.737162	0.000002	1.853388	0.000007	1.097481	0.000008
SSB2f (repeat)	0.321716	0.000009	0.108881	0.000005	0.737165	0.000005	1.853563	0.000024	1.097612	0.00002
Mean	0.321771	0.000003	0.108914	0.000001	0.737165	0.000002	1.85341	0.000008	1.097524	0.000008
μ(ppm)	21		146.1		27.3		−24.7		−39.2	
$\pm 2\sigma$(ppm)	206.2		389		3.9		109.4		108.3	
A2	0.321792	0.000002	0.108919	0.000001	0.737151	0.000002	1.853333	0.000006	1.097486	0.000007
μ(ppm)	117.2		237.5		10.7		−72.2		−76.8	

References

[1]. Poths H, Schmitt-Strecker S, Begemann F, On the isotopic composition of ruthenium in the Allende and Leoville carbonaceous chondrites, Geochim. Cosmochim. Acta 51 (1987) 1143–1149.

[2]. Kano N, Yamakoshi K, Matsuzaki H, Nogami K, Chemical and isotopic compositions in acid residues from three meteorites, Proc. NIPR Symp. Antarct. Meteor 6 (1993) 325–337.

[3]. Yin Q, Jagoutz E, Wänke H, Re-search for extinct ^{99}Tc and ^{98}Tc in the early solar system, Meteoritics 27 (1992) 310.

[4]. Savina MR, Davis AM, Tripa CE, Pellin MJ, Gallino R, Lewis RS, Amari S, Extinct technetium in silicon carbide stardust grains: implications for stellar nucleosynthesis, Science 303 (2004) 649–652. [PubMed: 14752154]

[5]. Fujii T, Moynier F, Telouk P, Albarède, Mass-independent isotope fractionation of molybdenum and ruthenium and the origin of isotopic anomalies in Murchison, Astrophys. J 647 (2006) 1506–1516.

[6]. Chen JH, Papanastassiou DA, Wasserburg GJ, Ruthenium endemic isotope effects in chondrites and differentiated meteorites, Geochim. Cosmochim. Acta 74 (2010) 3852–3862.

[7]. Fischer-Gödde M, Burkhardt C, Kruijer TS, Kleine T, Ru isotope heterogeneity in the solar protoplanetary disk, Ru isotope heterogeneity in the solar proto-planetary disk, Geochim. Cosmochim. Acta 168 (2015) 151–171.

[8]. Lodders K, Fegley B, The Planetary Scientist's Companion, Oxford University Press, 1998.

[9]. Hidaka H, Technetium in cosmo- and geochemical fields, J. Nucl. Radiochem. Sci 6 (2005) 249–252.

[10]. Bermingham KR, Walker RJ, Puchtel IS, O'Driscoll B, Probing terrestrial mantle evolution using Ru isotopes, in: Abstract VD-2796, Fall Meeting, AGU, San Francisco, CA, 9–13 12, 2013.

[11]. Walker RJ, Bermingham KR, Liu J, Puchtel IS, Touboul M, Worsham EA, In search of late-stage planetary building blocks, Chem. Geol 411 (2015) 125–142.

[12]. Norman MD, Bennett VC, Ryder G, Targeting the impactors: siderophile element signatures of lunar impact melts from Serenitatis, Earth Planet. Sci. Lett 202 (2002) 217–228.

[13]. Huang M, Liu Y, Masuda A, Accurate measurement of ruthenium isotopes by negative thermal ionization mass spectrometry, Anal. Chem 68 (1996) 841–844. [PubMed: 21619180]

[14]. Becker H, Dalpe C, Walker RJ, High-precision Ru isotopic measurements by multicollector ICP-MS, Analyst 127 (2002) 775–780. [PubMed: 12146910]

[15]. O'Driscoll B, Day JMD, Walker RJ, Daly JS, McDonough WF, Piccoli PM, Chemical heterogeneity in the upper mantle recorded by peridotities and chromitites from the Shetland Ophiolite Complex, Scotland, Earth Planet. Sci. Lett 333–334 (2012) 226–237.

[16]. Walker RJ, Brandon AD, Bird JM, Piccoli PM, McDonough WF, Ash RD, ^{187}Os-^{186}Os systematics of Os-Ir-Ru alloy grains from southwestern Oregon, Earth Planet. Sci. Lett 230 (2005) 211–226.

[17]. Walker RJ, McDonough WF, Honesto J, Chabot NL, McCoy TJ, Ash RD, Bellucci JJ, Modeling fractional crystallization of group IVB iron meteorites, Geochim. Cosmochim. Acta 72 (2008) 2198–2216.

[18]. Shirey SB, Walker RJ, Carius tube digestion for low-blank rhenium-osmium analysis, Anal. Chem 34 (1995) 2136–2141.

[19]. O'Neil MJ (Ed.), The Merck Index: An Encyclopedia of Chemicals, Drugs, and Biologicals, Merck Research Laboratories, 2006.

[20]. Rehkämper M, Halliday AN, Development and application of new ion-exchange techniques for the separation of the platinum group and other siderophile elements from geological samples, Talanta 44 (1997) 663–672. [PubMed: 18966788]

[21]. Seddon EA, Seddon KR, The Chemistry of Ruthenium, Elsevier Science Publishers, 1984.

[22]. Strelow FWE, An ion exchange selectivity scale of cations based on equilibrium distribution coefficients, Anal. Chem 32 (1960) 1185–1188.

[23]. Roy-Barman M, Mesure du rapport ^{187}Os/^{186}Os dans les basaltes et les peridotites: Contribution à la systématique ^{187}Re-^{187}Os dans le manteau (Thesis), Université de Paris VII, 1993.

[24]. Birck JL, Roy-Barman M, Capmas F, Re-Os isotopic measurements at the femtomole level in natural samples, Geostand. Newsl 21 (1997) 19–27.

[25]. Chen C, Sharma M, High precision and high sensitivity measurements of osmium in seawater, Anal. Chem 81 (2009) 5400–5406. [PubMed: 19499926]

[26]. Heumann KG, Eisenhut S, Gallus S, Hebeda EH, Nusko R, Vengosh A, Recent developments in thermal ionization mass spectrometric techniques for isotope analysis: a review, Analyst 120 (1985) 1291–1299.

[27]. Creaser RA, Papanastassiou DA, Wasserburg GJ, Negative thermal ion mass spectrometry of osmium, rhenium and iridium, Geochim. Cosmochim. Acta 55 (1991) 397–440.

[28]. Völkening J, Walczyk T, Heumann K, Osmium isotope ratio determinations by negative thermal ionization mass spectrometry, Int. J. Mass Spectrom. Ion Processes 105 (1991) 147–159.

[29]. Koornneef JM, Bouman C, Schwieters JB, Davies GR, Use of 10^{12} ohm current amplifiers in Sr and Nd isotope analyses by TIMS for application to sub-nanogram samples, J. Anal. At. Spectrom 28 (2013) 749–754.

[30]. Russell WA, Papanastassiou DA, Tombrello TA, Ca isotope fractionation in the Earth and other solar system materials, Geochim. Cosmochim. Acta 42 (1978) 1075–1090.

[31]. Yin Q, N-TIMS technique for the Re-Os and Ru isotopic systems and its applications to selected geochemical and cosmochemical problems (Thesis), der Johannes Gutenberg-Universität Mainz, 1995.

[32]. Nier AO, A redetermination of the relative abundances of the isotopes of carbon, nitrogen, oxygen, argon, and potassium, Phys. Rev 77 (1950) 789–793.

[33]. Burbidge EM, Burbidge GR, Fowler WA, Hoyle F, Synthesis of the elements in stars, Rev. Mod. Phys 29 (1957) 547–650.

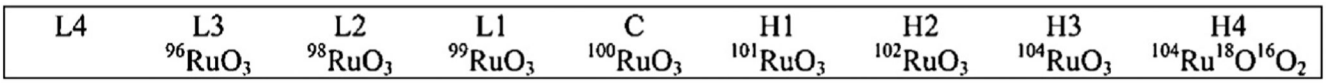

Fig. 1.
Faraday cup configuration for Ru isotope measurements.

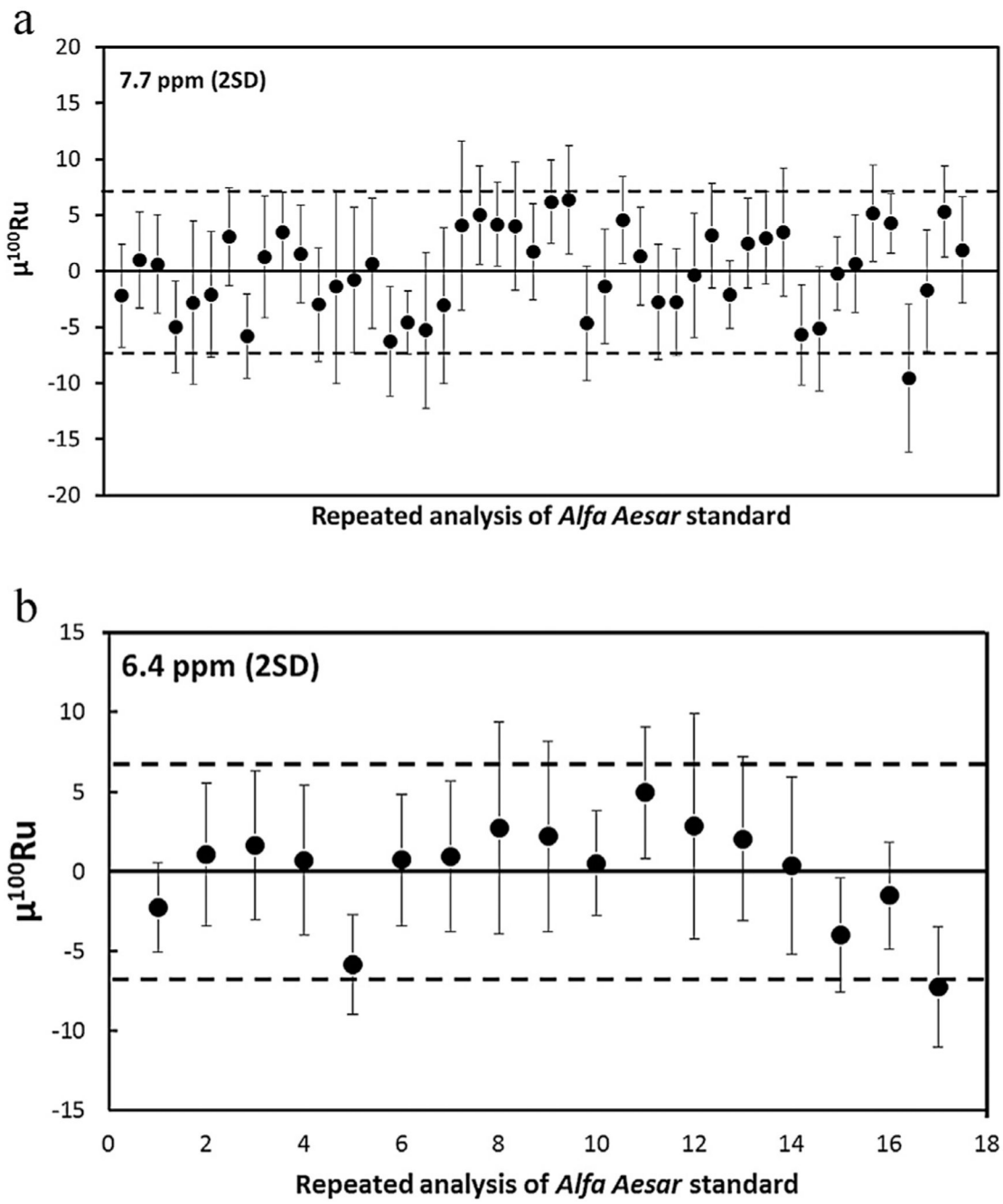

Fig. 2.

(a) Long-term (8 month) external reproducibility of $^{100}Ru/^{101}Ru$ in $\mu^{100}Ru$ units for 48 repeated analyses of 1000 ng Ru *Alfa Aesar* standard solution correcting for oxide interferences using an assumed oxygen isotope composition [32] and correction for mass fractionation using $^{99}Ru/^{101}Ru = 0.745075$. Error bars are the 2SE of each analysis. See Table 2 for details. (b) Short-term (1 month) external reproducibility of $^{100}Ru/^{101}Ru$ in $\mu^{100}Ru$ units for 17 repeated analyses of 1000 ng Ru Alfa Aesar standard solution, after correction for oxide interferences using a line-by-line measured oxygen isotope composition

and correction for mass fractionation using $^{99}Ru/^{101}Ru = 0.745075$. Error bars are the 2SE of each analysis. See Table 3 for details.

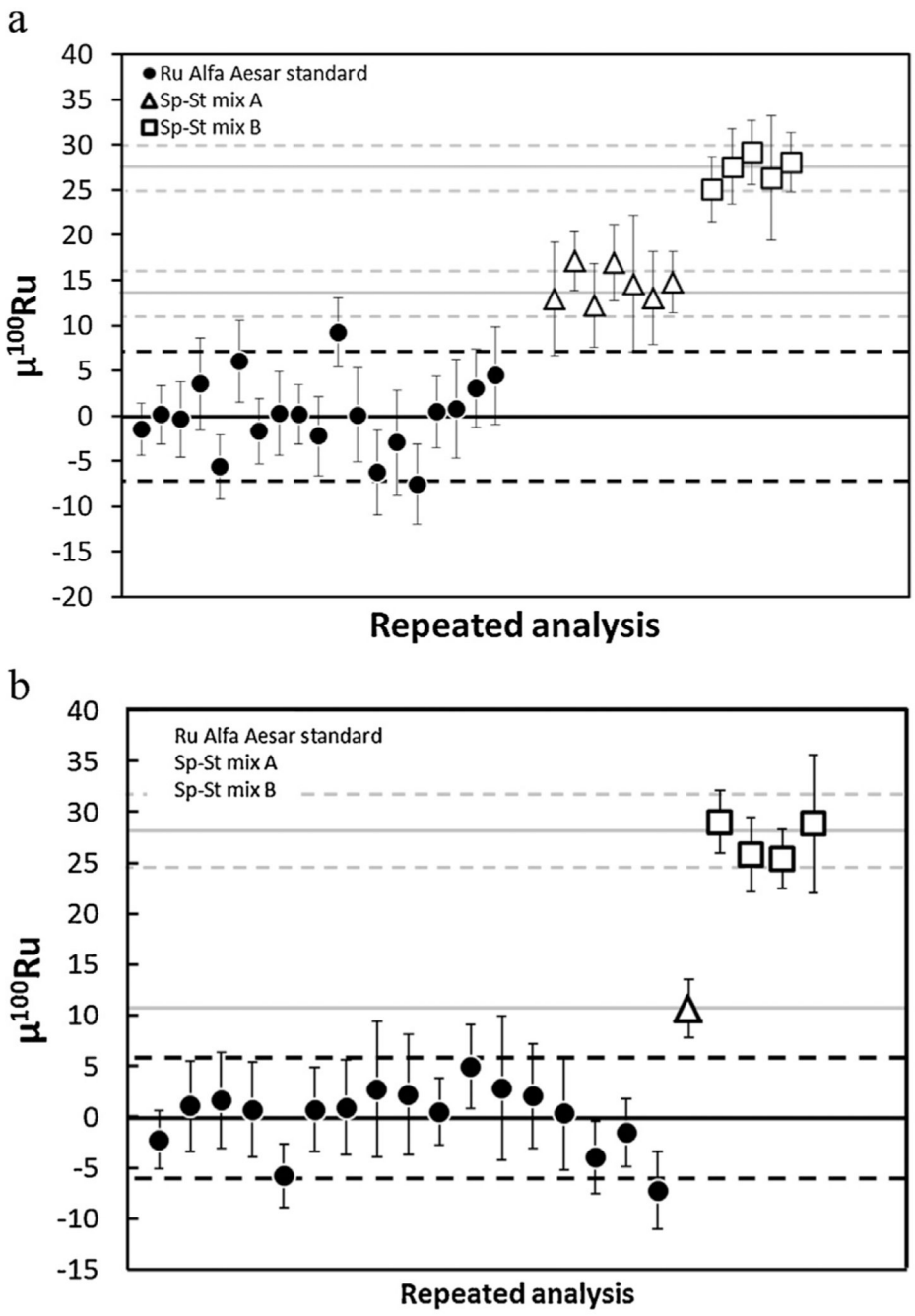

Fig. 3.

(a) $^{100}Ru/^{101}Ru$ ratios in $\mu^{100}Ru$ units for repeated analyses of standard-spike mixes (A and B) and Ru *Alfa Aesar* standard solution (see EA5 for details). Error bars are the 2SE of each analysis. These data have been corrected using an assumed oxygen isotope composition [32] and correction for mass fractionation using $^{99}Ru/^{101}Ru = 0.745075$ and the isotopic species. Spike-standard mix A shows a ~15 ppm ^{100}Ru positive anomaly, identical within analytical uncertainties to the gravimetric prediction (+14.9 ppm). Spike-standard mix B shows a ~30 ppm ^{100}Ru positive anomaly, identical within analytical uncertainties to the gravimetric

prediction (+29.3 ppm). (b) $^{100}Ru/^{101}Ru$ ratios in $\mu^{100}Ru$ units for repeated analyses of standard-spike mixes (A and B) and Ru *Alfa Aesar* standard solution (see EA5 for details). Error bars are the 2SE of each analysis. These data have been corrected using a line-by-line measured oxygen isotope composition and correction for mass fractionation using $^{99}Ru/^{101}Ru = 0.745075$ and the isotopic species. Spike-standard mix A and mix B are identical within analytical uncertainties to the gravimetric prediction (+14.9 ppm and +29.3 ppm, respectively).

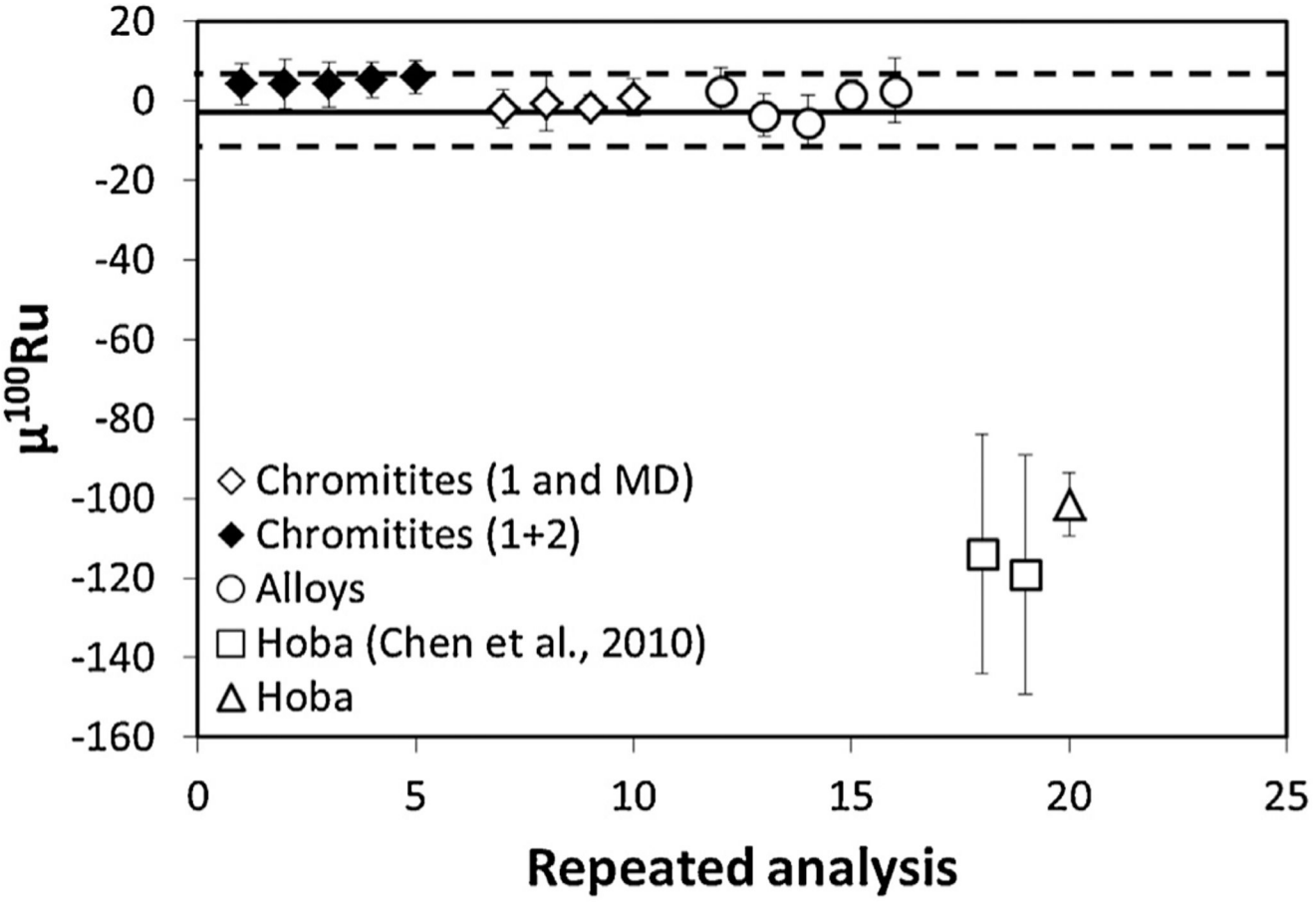

Fig. 4.

$^{100}Ru/^{101}Ru$ ratios in $\mu^{100}Ru$ units for repeated analyses of Shetland ophiolite chromitites that have been processed through 1° and 2° columns and microdistillation (filled symbols) and chromitites processed through 1° and microdistillation (open diamonds). The chromitites have identical compositions to the unprocessed *Alfa Aesar* standard within analytical uncertainties. Also shown are the $^{100}Ru/^{101}Ru$ ratios in $\mu^{100}Ru$ units for repeated analyses of Os-Ir-Ru alloys from the Josephine ophiolite, Oregon, that have been purified by microdistillation. The alloy grains have an identical composition to the *Alfa Aesar* standard within analytical uncertainties. The $^{100}Ru/^{101}Ru$ ratios in $\mu^{100}Ru$ units for repeated analyses of Hoba (IVB) has the same isotopic composition as reported by [6] within analytical error. These data have been corrected using an assumed oxygen isotope composition [32] and correction for mass fractionation using $^{99}Ru/^{101}Ru = 0.745075$ and the isotopic species (see Table 4 for details).

Table 1

Ion exchange chromatography procedure for Ru isolation and purification.

Acid	Volume (ml)	Step
1° cation column: 2–4 *Biorad* columns filled with 10 ml of pre-cleaned AG50WX8 (200–400 mesh)		
Milli-Q water	20	Resin cleaning
6M HCl	10 + 10 + 10 + 10	Resin cleaning
Milli-Q water	20	Resin cleaning
0.15 M HCl	10	Backwash
0.15 M HCl	10	Equilibration
0.15 M HCl	2.5	Load
0.15 M HCl	1 + 1 +1 + 5	Rinse HSE
6 M HCl	1 + 1 + 1 + 27	Rinse matrix
6 M HCl	10 + 10 + 10 + 10 + 10 + 10	Resin cleaning
Milli-Q water	20	Resin cleaning
2° anion column: 1 *Biorad* column filled with 3.8 ml of pre-cleaned AG1X8 (200–400 mesh)		
Milli-Q water	10	Resin cleaning
Concentrated HNO3	10 + 10	Resin cleaning
Milli-Q water	5	Resin cleaning
Concentrated HCl	10	Resin cleaning
Milli-Q water	5	Resin cleaning
1 M HCl	3	Backwash
1 M HCl	4	Equilibration
1 M HCl	1	Load
0.5 M HCl	2	Matrix, Mo
0.8 M HNO3	0.5	Matrix, Mo
0.8 M HNO3	5	Zn, Cd, Mo
8 M HNO3	10	Ru, Re
Concentrated HNO3	4	Ru, Re
Concentrated HNO3	10	Pt, Ir
11 M HCl	2	Pt, Ir, Ag
11 M HCl	8	Pd
Concentrated HNO3	5	Pd

Table 2

Results for the long term (8 month) Ru *Alfa Aesar* standard. These data have been corrected using an assumed oxygen isotope composition [32] and correction for mass fractionation using $^{99}Ru/^{101}Ru = 0.745075$ and the isotopic species.

	$^{96/101}$Ru	2SE	$^{98/101}$Ru	2SE	$^{100/101}$Ru	2SE	$^{102/101}$Ru	2SE	$^{104/101}$Ru	2SE
Ru std 01	0.321861	0.000004	0.108969	0.000002	0.737112	0.000003	1.853136	0.000010	1.097470	0.000011
Ru std 02	0.321857	0.000004	0.108969	0.000002	0.737114	0.000003	1.853161	0.000010	1.097477	0.000010
Ru std 03	0.321832	0.000004	0.108956	0.000002	0.737114	0.000003	1.853160	0.000010	1.097425	0.000011
Ru std 04	0.321843	0.000004	0.108968	0.000002	0.737110	0.000003	1.853144	0.000009	1.097446	0.000010
Ru std 05	0.321858	0.000007	0.108975	0.000004	0.737111	0.000005	1.853169	0.000016	1.097473	0.000017
Ru std 06	0.321844	0.000005	0.108975	0.000003	0.737112	0.000004	1.853140	0.000012	1.097445	0.000014
Ru std 07	0.321863	0.000004	0.108977	0.000002	0.737115	0.000003	1.853121	0.000010	1.097444	0.000011
Ru std 08	0.321847	0.000003	0.108972	0.000002	0.737109	0.000003	1.853132	0.000008	1.097432	0.000009
Ru std 09	0.321837	0.000005	0.108966	0.000003	0.737114	0.000004	1.853143	0.000011	1.097453	0.000012
Ru std 10	0.321870	0.000003	0.108967	0.000002	0.737116	0.000003	1.853166	0.000008	1.097513	0.000009
Ru std 11	0.321848	0.000004	0.108944	0.000002	0.737114	0.000003	1.853242	0.000010	1.097536	0.000011
Ru std 12	0.321871	0.000005	0.108965	0.000002	0.737111	0.000004	1.853214	0.000011	1.097563	0.000012
Ru std 13	0.321870	0.000008	0.108966	0.000004	0.737112	0.000006	1.853166	0.000018	1.097518	0.000019
Ru std 14	0.321857	0.000006	0.108973	0.000003	0.737113	0.000005	1.853175	0.000014	1.097532	0.000015
Ru std 15	0.321857	0.000006	0.108954	0.000003	0.737114	0.000004	1.853209	0.000013	1.097535	0.000014
Ru std 16	0.321855	0.000005	0.108958	0.000003	0.737109	0.000004	1.853193	0.000011	1.097499	0.000012
Ru std 17	0.321857	0.000002	0.108961	0.000001	0.737110	0.000002	1.853200	0.000006	1.097518	0.000007
Ru std 18	0.321874	0.000007	0.108967	0.000004	0.737109	0.000005	1.853173	0.000016	1.097472	0.000017
Ru std 19	0.321872	0.000007	0.108963	0.000004	0.737111	0.000005	1.853177	0.000015	1.097492	0.000017
Ru std 20	0.321846	0.000007	0.108965	0.000004	0.737116	0.000006	1.853209	0.000016	1.097553	0.000018
Ru std 21	0.321856	0.000004	0.108955	0.000002	0.737117	0.000003	1.853175	0.000009	1.097491	0.000010
Ru std 22	0.321846	0.000003	0.108951	0.000002	0.737116	0.000003	1.853223	0.000008	1.097518	0.000009
Ru std 23	0.321860	0.000005	0.108958	0.000003	0.737116	0.000004	1.853197	0.000012	1.097513	0.000013
Ru std 24	0.321853	0.000004	0.108962	0.000002	0.737115	0.000003	1.853188	0.000009	1.097501	0.000010
Ru std 25	0.321863	0.000004	0.108967	0.000002	0.737118	0.000003	1.853167	0.000008	1.097501	0.000009
Ru std 26	0.321855	0.000004	0.108961	0.000002	0.737118	0.000004	1.853212	0.000011	1.097540	0.000011
Ru std 27	0.321859	0.000005	0.108960	0.000002	0.737110	0.000004	1.853190	0.000011	1.097520	0.000012

	$^{96/101}$Ru	2SE	$^{98/101}$Ru	2SE	$^{100/101}$Ru	2SE	$^{102/101}$Ru	2SE	$^{104/101}$Ru	2SE
Ru std 28	0.321871	0.000005	0.108968	0.000003	0.737112	0.000004	1.853165	0.000012	1.097495	0.000013
Ru std 29	0.321867	0.000003	0.108964	0.000002	0.737117	0.000003	1.853176	0.000008	1.097508	0.000009
Ru std 30	0.321855	0.000004	0.108959	0.000002	0.737114	0.000003	1.853198	0.000010	1.097497	0.000011
Ru std 31	0.321857	0.000005	0.108956	0.000002	0.737111	0.000004	1.853195	0.000011	1.097516	0.000012
Ru std 32	0.321869	0.000004	0.108970	0.000002	0.737111	0.000004	1.853139	0.000011	1.097484	0.000011
Ru std 33	0.321860	0.000005	0.108963	0.000003	0.737113	0.000004	1.853177	0.000012	1.097506	0.000013
Ru std 34	0.321861	0.000004	0.108969	0.000002	0.737116	0.000003	1.853152	0.000010	1.097464	0.000011
Ru std 35	0.321864	0.000003	0.108972	0.000001	0.737112	0.000002	1.853137	0.000007	1.097467	0.000007
Ru std 36	0.321864	0.000004	0.108979	0.000002	0.737115	0.000003	1.853128	0.000009	1.097470	0.000010
Ru std 37	0.321871	0.000004	0.108975	0.000002	0.737115	0.000003	1.853128	0.000009	1.097482	0.000010
Ru std 38	0.321865	0.000005	0.108968	0.000003	0.737116	0.000004	1.853157	0.000013	1.097475	0.000013
Ru std 39	0.321862	0.000004	0.108971	0.000002	0.737109	0.000003	1.853152	0.000010	1.097506	0.000011
Ru std 40	0.321853	0.000005	0.108958	0.000003	0.737109	0.000004	1.853193	0.000012	1.097515	0.000013
Ru std 41	0.321862	0.000003	0.108963	0.000001	0.737113	0.000002	1.853159	0.000007	1.097485	0.000008
Ru std 42	0.321866	0.000004	0.108966	0.000002	0.737114	0.000003	1.853145	0.000011	1.097480	0.000012
Ru std 43	0.321842	0.000004	0.108952	0.000002	0.737117	0.000003	1.853221	0.000010	1.097502	0.000011
Ru std 44	0.321848	0.000003	0.108957	0.000001	0.737116	0.000002	1.853212	0.000007	1.097508	0.000007
Ru std 45	0.321856	0.000006	0.108967	0.000003	0.737106	0.000005	1.853139	0.000014	1.097468	0.000015
Ru std 46	0.321859	0.000005	0.108972	0.000003	0.737112	0.000004	1.853146	0.000012	1.097477	0.000013
Ru std 47	0.321848	0.000004	0.108958	0.000002	0.737117	0.000003	1.853188	0.000009	1.097487	0.000010
Ru std 48	0.321846	0.000004	0.108956	0.000002	0.737115	0.000004	1.853205	0.000011	1.097497	0.000012
Mean	0.321857	0.000005	0.108964	0.000002	0.737113	0.000004	1.853173	0.000011	1.097493	0.000012
$\pm 2\sigma$ (ppm)	60.5		136.9		7.7		32.0		55.4	

Table 3

Results for the short term (1 month) Ru *Alfa Aesar* standard using different correction schemes as indicated. All data have been corrected for mass fractionation using $^{99}Ru/^{101}Ru = 0.745075$.

	$^{96/101}Ru$	2SE	$^{98/101}Ru$	2SE	$^{100/101}Ru$	2SE	$^{102/101}Ru$	2SE	$^{104/101}Ru$	2SE
Corrected using an assumed oxygen isotope composition [32]										
Ru std 01	0.321799	0.000003	0.108933	0.000002	0.737143	0.000002	1.853247	0.000007	1.097404	0.000007
Ru std 02	0.321827	0.000004	0.108947	0.000002	0.737146	0.000003	1.853231	0.000010	1.097448	0.000011
Ru std 03	0.321815	0.000005	0.108945	0.000002	0.737147	0.000003	1.853230	0.000011	1.097450	0.000012
Ru std 04	0.321800	0.000004	0.108937	0.000002	0.737148	0.000003	1.853259	0.000011	1.097440	0.000012
Ru std 05	0.321818	0.000003	0.108941	0.000001	0.737141	0.000002	1.853234	0.000007	1.097435	0.000007
Ru std 06	0.321801	0.000003	0.108945	0.000002	0.737149	0.000003	1.853215	0.000009	1.097398	0.000009
Ru std 07	0.321826	0.000004	0.108945	0.000002	0.737148	0.000003	1.853221	0.000010	1.097445	0.000011
Ru std 08	0.321813	0.000006	0.108936	0.000003	0.737149	0.000005	1.853250	0.000014	1.097441	0.000016
Ru std 09	0.321797	0.000007	0.108923	0.000004	0.737145	0.000005	1.853325	0.000016	1.097462	0.000017
Ru std 10	0.321804	0.000005	0.108931	0.000003	0.737145	0.000004	1.853282	0.000013	1.097453	0.000014
Ru std 11	0.321790	0.000004	0.108919	0.000002	0.737149	0.000003	1.853306	0.000010	1.097454	0.000010
Ru std 12	0.321823	0.000007	0.108938	0.000004	0.737151	0.000005	1.853277	0.000018	1.097508	0.000020
Ru std 13	0.321812	0.000005	0.108935	0.000002	0.737151	0.000004	1.853287	0.000011	1.097501	0.000012
Ru std 14	0.321802	0.000005	0.108934	0.000003	0.737150	0.000004	1.853284	0.000011	1.097466	0.000012
Ru std 15	0.321817	0.000003	0.108941	0.000002	0.737144	0.000003	1.853255	0.000009	1.097463	0.000008
Ru std 16	0.321819	0.000003	0.108934	0.000002	0.737147	0.000002	1.853309	0.000008	1.097507	0.000008
Ru std 17	0.321813	0.000003	0.108939	0.000002	0.737142	0.000003	1.853267	0.000009	1.097477	0.000009
Mean	0.321810		0.108937		0.737147		1.853263		1.097456	
$\pm 2\sigma$(ppm)	67.7		138.0		8.2		35.1		56.2	
Corrected using a line-by-line measured oxygen isotope composition										
Ru std 01	0.321777	0.000003	0.108915	0.000001	0.737142	0.000002	1.853326	0.000007	1.097448	0.000008
Ru std 02	0.321794	0.000004	0.108922	0.000002	0.737144	0.000003	1.853349	0.000010	1.097515	0.000011
Ru std 03	0.321784	0.000005	0.108921	0.000002	0.737145	0.000003	1.853343	0.000011	1.097511	0.000012
Ru std 04	0.321727	0.000005	0.108882	0.000003	0.737144	0.000003	1.853521	0.000012	1.097590	0.000013
Ru std 05	0.321778	0.000003	0.108910	0.000001	0.737139	0.000002	1.853375	0.000007	1.097515	0.000007
Ru std 06	0.321724	0.000004	0.108885	0.000002	0.737144	0.000003	1.853495	0.000010	1.097557	0.000010

	$^{96/101}$Ru	2SE	$^{98/101}$Ru	2SE	$^{100/101}$Ru	2SE	$^{102/101}$Ru	2SE	$^{104/101}$Ru	2SE
Ru std 07	0.321762	0.000004	0.108897	0.000002	0.737144	0.000003	1.853448	0.000010	1.097574	0.000011
Ru std 08	0.321748	0.000008	0.108886	0.000005	0.737145	0.000005	1.853484	0.000021	1.097573	0.000019
Ru std 09	0.321790	0.000006	0.108918	0.000003	0.737145	0.000004	1.853346	0.000017	1.097475	0.000017
Ru std 10	0.321780	0.000004	0.108913	0.000002	0.737144	0.000002	1.853371	0.000009	1.097502	0.000009
Ru std 11	0.321755	0.000004	0.108893	0.000002	0.737147	0.000003	1.853436	0.000010	1.097527	0.000011
Ru std 12	0.321734	0.000008	0.108867	0.000004	0.737145	0.000005	1.853610	0.000021	1.097694	0.000022
Ru std 13	0.321715	0.000005	0.108859	0.000003	0.737145	0.000004	1.853650	0.000013	1.097708	0.000013
Ru std 14	0.321707	0.000006	0.108859	0.000003	0.737144	0.000004	1.853629	0.000016	1.097658	0.000014
Ru std 15	0.321764	0.000003	0.108901	0.000002	0.737140	0.000003	1.853449	0.000008	1.097572	0.000009
Ru std 16	0.321743	0.000003	0.108875	0.000002	0.737142	0.000002	1.853585	0.000009	1.097664	0.000009
Ru std 17	0.321745	0.000003	0.108888	0.000002	0.737138	0.000003	1.853517	0.000009	1.097618	0.000009
Mean	0.321755		0.108894		0.737143		1.853467		1.097571	
$\pm 2\sigma$ (ppm)	168.4		386.9		6.4		115.6		139.5	

Int J Mass Spectrom. Author manuscript; available in PMC 2019 February 01.

Table 4

Results for the Os-Ir-Ru alloys, chromitites, and Hoba (IVB) processed through chemistry (as indicated). These data have been corrected using an assumed oxygen isotope composition [32] and correction for mass fractionation using $^{99}Ru/^{101}Ru = 0.745075$ and the isotopic species. Samples have been compared to the Ru *Alfa Aesar* standard analyzed during the respective analytical campaign.

	$^{96/101}$Ru	2SE	$^{98/101}$Ru	2SE	$^{100/101}$Ru	2SE	$^{102/101}$Ru	2SE	$^{104/101}$Ru	2SE
Os-Ir-Ru alloys processed through microdistillation										
M3_6	0.321847	0.000005	0.108959	0.000003	0.737097	0.000004	1.853133	0.000012	1.097506	0.000013
μ(ppm)	36.4		−24.0		7.4		10.3		53.3	
M8_02	0.321855	0.000006	0.108958	0.000003	0.737089	0.000005	1.853122	0.000013	1.097461	0.000014
μ(ppm)	60.4		−32.1		−4.5		4.0		12.2	
L5_3a	0.321857	0.000005	0.108965	0.000003	0.737094	0.000004	1.853077	0.000012	1.097434	0.000013
L5_3b	0.321840	0.000005	0.108946	0.000003	0.737089	0.000004	1.853170	0.000012	1.097495	0.000013
L5_3c	0.321840	0.000006	0.108962	0.000004	0.737088	0.000005	1.853113	0.000015	1.097472	0.000016
L5_3d	0.321839	0.000003	0.108961	0.000002	0.737093	0.000003	1.853079	0.000009	1.097412	0.000009
L5_3e	0.321847	0.000007	0.108965	0.000004	0.737094	0.000006	1.853162	0.000017	1.097492	0.000019
Mean	0.321845	0.000005	0.108960	0.000003	0.737092	0.000004	1.853120	0.000013	1.097461	0.000014
μ(ppm)	29.4		−16.2		−0.5		3.3		12.5	
±2σ(ppm)	45.5		142.5		7.56		47.7		66.5	
Chromitites processed through 1° + 2° columns & microdistillation										
C1	0.321845	0.000005	0.108950	0.000002	0.737116	0.000004	1.853221	0.000012	1.09750	0.000013
C2	0.321864	0.000006	0.108970	0.000003	0.737116	0.000005	1.853184	0.000014	1.097483	0.000015
C3a	0.321837	0.000005	0.108956	0.000002	0.737116	0.000004	1.853215	0.000013	1.097482	0.000014
C3b	0.321848	0.000004	0.108966	0.000002	0.737117	0.000003	1.853187	0.000010	1.097480	0.000011
C3c	0.321847	0.000004	0.108961	0.000002	0.737118	0.000003	1.853200	0.000009	1.097489	0.000010
Mean	0.321848	0.000005	0.108960	0.000002	0.737117	0.000004	1.853201	0.000012	1.097487	0.000013
Mean (ppm)	−28.9		−44.6		4.6		19.6		−0.1	
±2σ(ppm)	61.7		145.0		1.7		17.7		15.0	
Chromitites processed through 1° column & microdistillation										
C3_02a	0.321836	0.000005	0.108955	0.000002	0.737135	0.000004	1.853189	0.000011	1.097427	0.000012
C3_02b	0.321829	0.000006	0.108965	0.000003	0.737136	0.000005	1.853196	0.000015	1.097450	0.000014
C3_02c	0.321832	0.000003	0.108956	0.000001	0.737135	0.000002	1.853196	0.000007	1.097455	0.000007

	$^{96/101}$Ru	2SE	$^{98/101}$Ru	2SE	$^{100/101}$Ru	2SE	$^{102/101}$Ru	2SE	$^{104/101}$Ru	2SE
C3_02d	0.321840	0.000005	0.108960	0.000003	0.737137	0.000004	1.853205	0.000010	1.097475	0.000013
Mean	0.321834	0.000005	0.108959	0.000002	0.737135	0.000004	1.853197	0.000011	1.097452	0.000012
μ (ppm)	25.0		31.6		−0.9		4.2		13.4	
$\pm 2\sigma$ (ppm)	30.3		84.9		2.6		7.3		35.7	
Iron meteorite processed through 1° + 2° columns & microdistillation										
Hoba a	0.321883	0.000008	0.108985	0.000004	0.737033	0.000006	1.853117	0.000018	1.097542	0.000019
Hoba b	0.321873	0.000008	0.108977	0.000005	0.737029	0.000007	1.853074	0.000020	1.097534	0.000022
Mean	0.321878	0.000008	0.108981	0.000005	0.737031	0.000006	1.853096	0.000019	1.097538	0.000021
μ (ppm)	117.2		268.3		−116.9		−64.8		34.2	
$\pm 2\sigma$ (ppm)	45.4		99.2		7.5		32.1		10.1	
Lit. mean (ppm)[a]	57		43.5		−98.0		−27.5		24.5	
$\pm 2\sigma$ (ppm)	119		118		31		64		58	

[a] Data from [6].